

# Prostanoid induces premetastatic niche in regional lymph nodes

Fumihiro Ogawa,<sup>1,2</sup> Hideki Amano,<sup>1</sup> Koji Eshima,<sup>3</sup> Yoshiya Ito,<sup>1</sup> Yoshio Matsui,<sup>1,4</sup> Kanako Hosono,<sup>1</sup> Hidero Kitasato,<sup>5</sup> Akira Iyoda,<sup>6</sup> Kazuya Iwabuchi,<sup>3</sup> Yuji Kumagai,<sup>1,2</sup> Yukitoshi Satoh,<sup>4</sup> Shuh Narumiya,<sup>7</sup> and Masataka Majima<sup>1</sup>

<sup>1</sup>Department of Pharmacology, <sup>2</sup>Department of Clinical Research Center, <sup>3</sup>Department of Immunology, and <sup>4</sup>Department of Thoracic Surgery, Kitasato University School of Medicine, Kanagawa, Japan.

<sup>5</sup>Department of Microbiology, Kitasato University School of Allied Health Science, Kanagawa, Japan. <sup>6</sup>Department of Thoracic Surgery, Toho University School of Medicine, Tokyo, Japan.

<sup>7</sup>Department of Pharmacology, Kyoto University Graduate School of Medicine, Kyoto, Japan.

The lymphatic system is an important route for cancer dissemination, and lymph node metastasis (LNM) serves as a critical prognostic determinant in cancer patients. We investigated the contribution of COX-2-derived prostaglandin E<sub>2</sub> (PGE<sub>2</sub>) in the formation of a premetastatic niche and LNM. A murine model of Lewis lung carcinoma (LLC) cell metastasis revealed that COX-2 is expressed in DCs from the early stage in the lymph node subcapsular regions, and COX-2 inhibition markedly suppressed mediastinal LNM. Stromal cell-derived factor-1 (SDF-1) was elevated in DCs before LLC cell infiltration to the lymph nodes, and a COX-2 inhibitor, an SDF-1 antagonist, and a CXCR4 neutralizing antibody all reduced LNM. Moreover, LNM was reduced in mice lacking the PGE<sub>2</sub> receptor EP3, and stimulation of cultured DCs with an EP3 agonist increased SDF-1 production. Compared with WT CD11c<sup>+</sup> DCs, injection of EP3-deficient CD11c<sup>+</sup> DCs dramatically reduced accumulation of SDF-1<sup>+</sup>CD11c<sup>+</sup> DCs in regional LNs and LNM in LLC-injected mice. Accumulation of Tregs and lymph node lymphangiogenesis, which may influence the fate of metastasized tumor cells, was also COX-2/EP3-dependent. These results indicate that DCs induce a premetastatic niche during LNM via COX-2/EP3-dependent induction of SDF-1 and suggest that inhibition of this signaling axis may be an effective strategy to suppress premetastatic niche formation and LNM.

## Introduction

It is widely accepted that many tumors tend to metastasize to specific organs (1). The mechanisms that guide tumor cells to specific tissues are largely unknown, although recent evidence suggests that it may involve molecular differences inherent in the tumor cells themselves, modulated by the activities of immune cells, hematopoietic cells, and other tissue components. Lymph node metastasis (LNM) is a critical prognostic factor in cancer patients, and lymphatic vessels serve as an important route for the spread of cancer cells (1). Paget reported that tumor cells might prepare the lymph nodes for their future arrival, giving a new interpretation to the seed-and-soil hypothesis (2). The formation of a premetastatic niche, suitable for the arrival of the first tumor cells, facilitates metastasis via the bloodstream (3, 4). However, data regarding the factors involved in lymph node premetastatic niche formation are limited (5). Tumor-associated lymphangiogenesis may enhance metastasis to the regional lymph nodes; however, the involvement of lymph node premetastatic niche formation in the metastatic process is unclear.

The cellular components involved in tumor cell metastasis to a predetermined location are largely unknown. However, Kaplan et al. (4) demonstrated that bone marrow-derived hematopoietic progenitor cells expressing VEGFR1 (also known as FLT1) home to

tumor-specific premetastatic sites and form cellular clusters before the arrival of tumor cells. Their findings demonstrated a requirement for VEGFR1<sup>+</sup> hematopoietic progenitors in the regulation of metastasis, and suggested that expression patterns of fibronectin and clusters positive for VEGFR1 and VLA-4 (also known as integrin  $\alpha_4\beta_1$ ) dictate organ-specific tumor spread. However, the involvement of other cellular components in premetastatic niche formation is largely unknown. Among the many cellular components within the tumor microenvironment, dendritic cells (DCs) exert profound effects on T cells (6). The mediators that regulate DC function may also modulate niche formation. Prostaglandin E<sub>2</sub> (PGE<sub>2</sub>) and the tryptophan-catabolizing enzyme indoleamine 2,3-dioxygenase (IDO) exert strong effects on the maturation and function of DCs (7). In addition, PGE<sub>2</sub> has been identified as a major immunosuppressive soluble factor present in the tumor microenvironment (8, 9). An important mechanism by which these DCs modulate T cell responses seems to be via PGE<sub>2</sub>-induced expression of IDO. Furthermore, a recent study reported that PGE<sub>2</sub> increased the immunosuppressive potential of regulatory T cells (Tregs) (10). We previously reported that COX-2-derived endogenous PGE<sub>2</sub> enhanced angiogenesis and lymphangiogenesis during tumor development and chronic inflammation (11, 12). Furthermore, PGE<sub>2</sub> enhances stromal tissue formation and tumor-associated angiogenesis mediated by tumor stromal chemokines (13). The function of a broad range of immune cells can be regulated by PGE<sub>2</sub>; however, the precise contributions of PGE<sub>2</sub> to LNM are not clear.

In this study, we show that endogenous COX-2-derived PGE<sub>2</sub> stimulated the EP3 receptor on DCs and upregulated the expression of stromal cell-derived factor-1 (SDF-1) in the subcapsular

**Authorship note:** Fumihiro Ogawa, Hideki Amano, and Koji Eshima contributed equally to this work.

**Conflict of interest:** The authors have declared that no conflict of interest exists.

**Submitted:** October 1, 2013; **Accepted:** August 21, 2014.

**Reference information:** *J Clin Invest.* 2014;124(11):4882–4894. doi:10.1172/JCI73530.

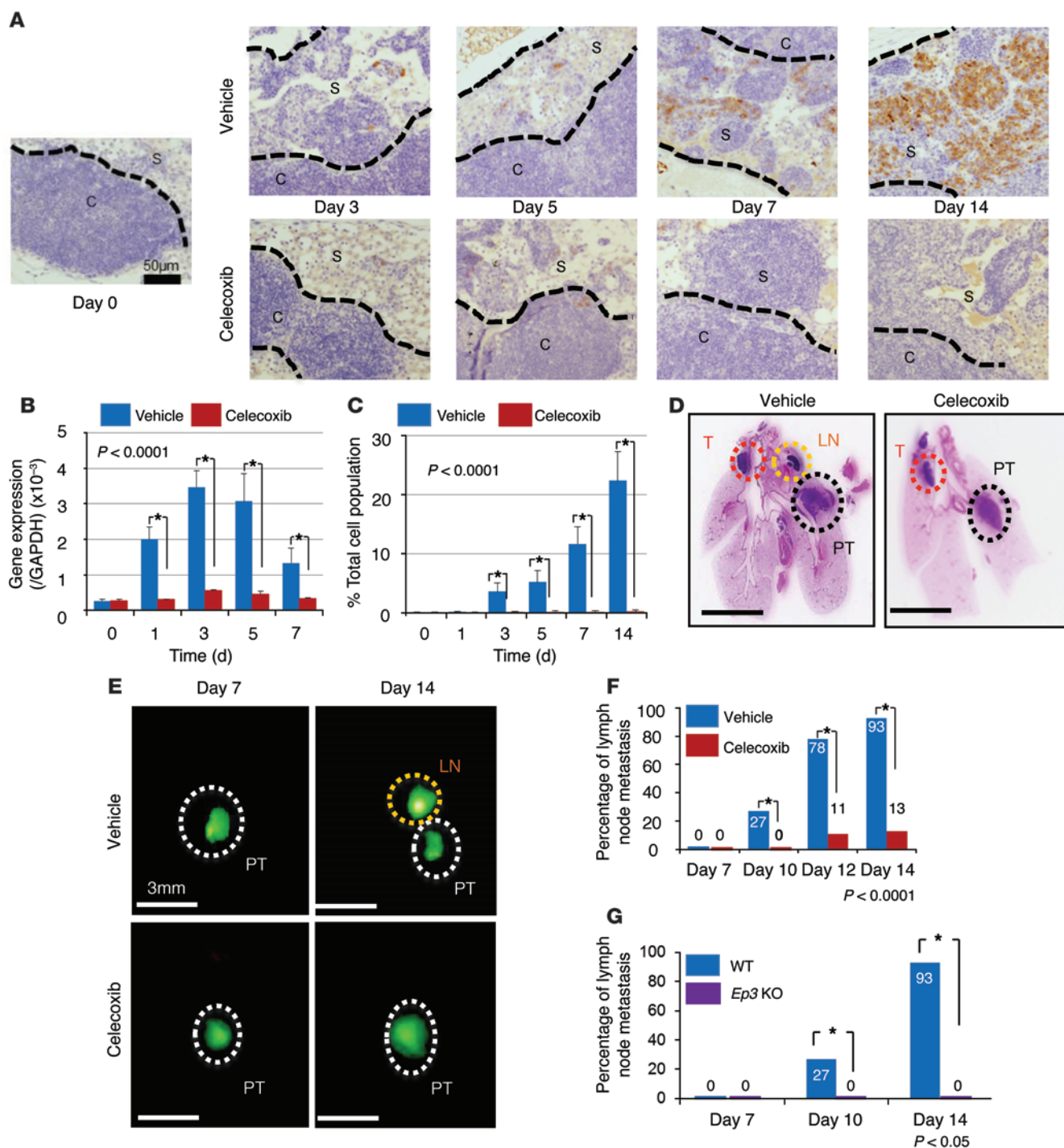


**Figure 1. COX-2 induction in regional lymph nodes and the effect of COX-2 inhibition on regional LNM.** (A) Immunohistochemical COX-2 staining of the regional lymph nodes after lung LLC cell implantation. In vehicle-treated mice, COX-2-positive cells were localized in the subcapsular regions. Celecoxib was given orally throughout the experimental period. Scale bar: 50  $\mu$ m. (B) RT-PCR analysis of *Cox2*. *Cox2* mRNA levels were significantly reduced in the celecoxib-treated group compared with the vehicle-treated group.  $n = 15$  per group.  $*P < 0.0001$  (ANOVA). (C) The percentage total cell population of COX-2-positive cells was significantly reduced in the celecoxib-treated group compared with the vehicle-treated group.  $n = 15$  per group.  $*P < 0.0001$  (ANOVA). (D) Loupe images by typical H&E staining obtained on day 10 after injection. Scale bars: 5 mm. (E) Fluorescence microscope images obtained after implantation of GFP-positive LLC cells into the lung. Scale bars: 3 mm. (F) Temporal changes in the percentage of regional LNM-positive mice. Metastasis in the vehicle-treated group was compared with that in the celecoxib-treated group.  $n = 15$  per group.  $*P < 0.0001$  ( $\chi^2$  test). (G) Percentage of regional LNM-positive mice. Metastasis was compared between *Ep3* KO mice and WT mice. WT,  $n = 15$ ; *Ep3* KO,  $n = 5$ .  $*P < 0.05$  ( $\chi^2$  test). Error bars indicate the mean  $\pm$  SD.  $N$  indicates the number of mice tested. S, subcapsular regions; C, cortex; PT, primary tumor; LN, lymph node; T, thymus.

regions of regional lymph nodes following Lewis lung carcinoma (LLC) cell injection. SDF-1 upregulation increased the accumulation of CXCR4<sup>+</sup> LLC cells and facilitated the formation of regional lymph node premetastatic niches. The accumulation of Tregs and lymph node lymphangiogenesis, both of which may influence the fate of metastasized tumor cells, were also COX-2/EP3-dependent. Thus, inhibitors of PGE<sub>2</sub>, together with SDF-1 receptor antagonists and EP3 antagonists, may be effective at suppressing premetastatic niche formation and LNM. These findings strongly suggest a novel function of PGE<sub>2</sub> in the formation of the lymph node premetastatic niche.

## Results

*Early expression of COX-2 in premetastatic regional lymph nodes and COX-2-derived PGE<sub>2</sub>-EP3 signaling enhances LNM.* To test the involvement of COX-2-derived PGE<sub>2</sub>, we injected GFP-transfected LLC cells ( $5.0 \times 10^4$  per  $10 \mu\text{l}$ ) directly into the lung under anesthesia. The inclusion of Matrigel prevented the occurrence of sudden death due to hemothorax or pneumothorax. The injected LLC cells formed tumors in the parenchyma of the lungs. There were no significant changes in tumor size in the mice treated with celecoxib (a COX-2 inhibitor) or vehicle at 10 days after the injection of LLC cells (Supplemental Figure 1A; supplemental material available online with this article; doi:10.1172/JCI73530DS1). However, COX-2-expressing cells were identified in the subcapsular region of the regional lymph nodes at 1 or 3 days after the LLC cell implantation (Figure 1, A and C). This was confirmed by analysis of mRNA levels in the lymph node tissues (Figure 1B). There was no obvious metastasis at 7 days (Figure 1, D and E). Regional LNM, which was established in vehicle-treated mice at 10, 12, and 14 days, was prevented by COX-2 inhibitor treatment (Figure 1, D-F). Moreover, the percentage of LNM-positive mice was significantly reduced by celecoxib treatment (Figure 1F). These results were confirmed by the RT-PCR results that GFP expressions in the regional lymph node were suppressed under COX-2 inhibition (Supplemental Figure 1B). Therefore, we injected only Matrigel without tumor to the left lung directly and analyzed regional lymph nodes by immunohistochemistry with COX-2 and CD11c. COX-2- and CD11c-positive cells slightly increased at subcapsular regions in the early phase after injection, but, thereafter, they did not increase more over time (Supplemental Figure 1C). COX-2 expression was also suppressed following celecoxib treatment (Figure 1, A-C). MTT assay showed that proliferation of LLC did not affect understimulation of COX-2 inhibitor (Supplemental Figure 1D). This result suggested that celecoxib did not affect tumor growth directly. We previously reported that EP3 signaling increased tumor cell growth and metastasis formation (11, 14). Therefore, we examined LNM formation in *Ep3* KO mice. The formation of LNM in *Ep3* KO mice at 14 days was significantly suppressed compared with that in WT mice (Figure 1G). These results suggested that COX-2-derived PGE<sub>2</sub>-EP3 signaling enhanced LNM after parenchymal injection of LLC cells.

*COX-2-dependent premetastatic niche formation in regional lymph nodes.* Stromal cell-derived factor-1 (SDF-1, CXCL12) and its receptor, CXCR4, play an important role in metastasis (15-17). Numerous studies show that CXCR4 is the major chemokine

receptor expressed in many types of cancer cells, and that the SDF-1/CXCR4 axis plays a major role in the survival, proliferation, migration, and adhesion of tumor cells (18-25).

Moreover, CXCR4-expressing cancer cells preferentially home to organs with high CXCL12 expression, such as the lung, liver, and bone marrow, via the blood and lymphatic system (26, 27).

In the present study, we examined the expression of CXCR4 in GFP-labeled LLC cells by immunofluorescence, and found that the large population of GFP-positive LLC cells were also positive for CXCR4 (Figure 2A). Next, we examined the expression of SDF-1, a ligand for CXCR4, in the regional lymph nodes following LLC cell injection. The expression of SDF-1 in vehicle-treated mice was significantly increased on days 3 and 5 compared with that in celecoxib-treated mice (Figure 2B). Prior to the arrival of the injected LLC cells, we observed increased accumulation of SDF-1-expressing cells in the subcapsular regions from 3 and 5 days. Many of these SDF-1-positive cells were also COX-2-positive (Figure 2C). Furthermore, the expression of *Cox2* and *Sdf1* in regional lymph nodes estimated by RT-PCR was consistent with immunohistochemistry (Supplemental Figure 2, A and B). Western blot analysis revealed that the expression of COX-2 in the regional lymph nodes was suppressed in the celecoxib-treated group and *Ep3* KO mice (Supplemental Figure 2C). At day 14, LLC cells preferentially accumulated in a COX-2-dependent manner in subcapsular regions rich in SDF-1/COX-2-double positive cells (Figure 2D). This finding suggested that COX-2-dependent SDF-1 induction increased metastasis to a predetermined location, specifically the subcapsular regions within the lymph node, and was crucial for the establishment of the lymph node premetastatic niche.

*The SDF-1/CXCR4 axis governs the accumulation of LLC cells in the lymph node premetastatic niche.* To determine whether the SDF-1/CXCR4 axis induces premetastatic niche formation, we injected a CXCR4 antagonist, AMD3100, following the injection of LLC cells. There was no significant difference in tumor size between vehicle- and AMD3100-treated mice during the experimental period (Figure 2E). However, LNM was completely suppressed in mice treated with AMD3100 or CXCR4 neutralizing antibody on day 10 and day 14 (Figure 2F).

Furthermore, the accumulation of SDF-1/COX-2-double positive cells in the regional lymph nodes (Supplemental Figure 2D) was suppressed in AMD3100-treated mice (Figure 2G). This reduction was also seen in *Ep3* KO mice (Figure 2H and Supplemental Figure 2D). These results suggested that LNM driven by COX-2/EP3 is highly dependent on the SDF-1/CXCR4 axis.

*COX-2-positive DCs accumulate in the lymph node premetastatic niche and produce SDF-1 via EP3 signaling.* To clarify the cellular components relevant to premetastatic niche formation, we examined the cell surface marker profiles of COX-2-expressing cells. We found that DC marker-positive cells accumulated in the subcapsular regions of the lymph nodes (Figure 3A). Among the DC markers, CD11c, which is a type I transmembrane protein, is highly expressed on most DCs. Furthermore, indoleamine 2,3-dioxygenase (IDO) is also considered to be a good marker for DCs, and PGE<sub>2</sub> was reported to induce IDO in tolerogenic DCs (28). In the present study, immunohistochemical analysis revealed that COX-2-positive cells were also positive for CD11c and IDO (Figure 3, A and B). The accumulation of CD11c- and IDO-positive cells was suppressed in celecoxib- or AMD3100-treated mice and in *Ep3* KO mice (Figure 3, C and D).

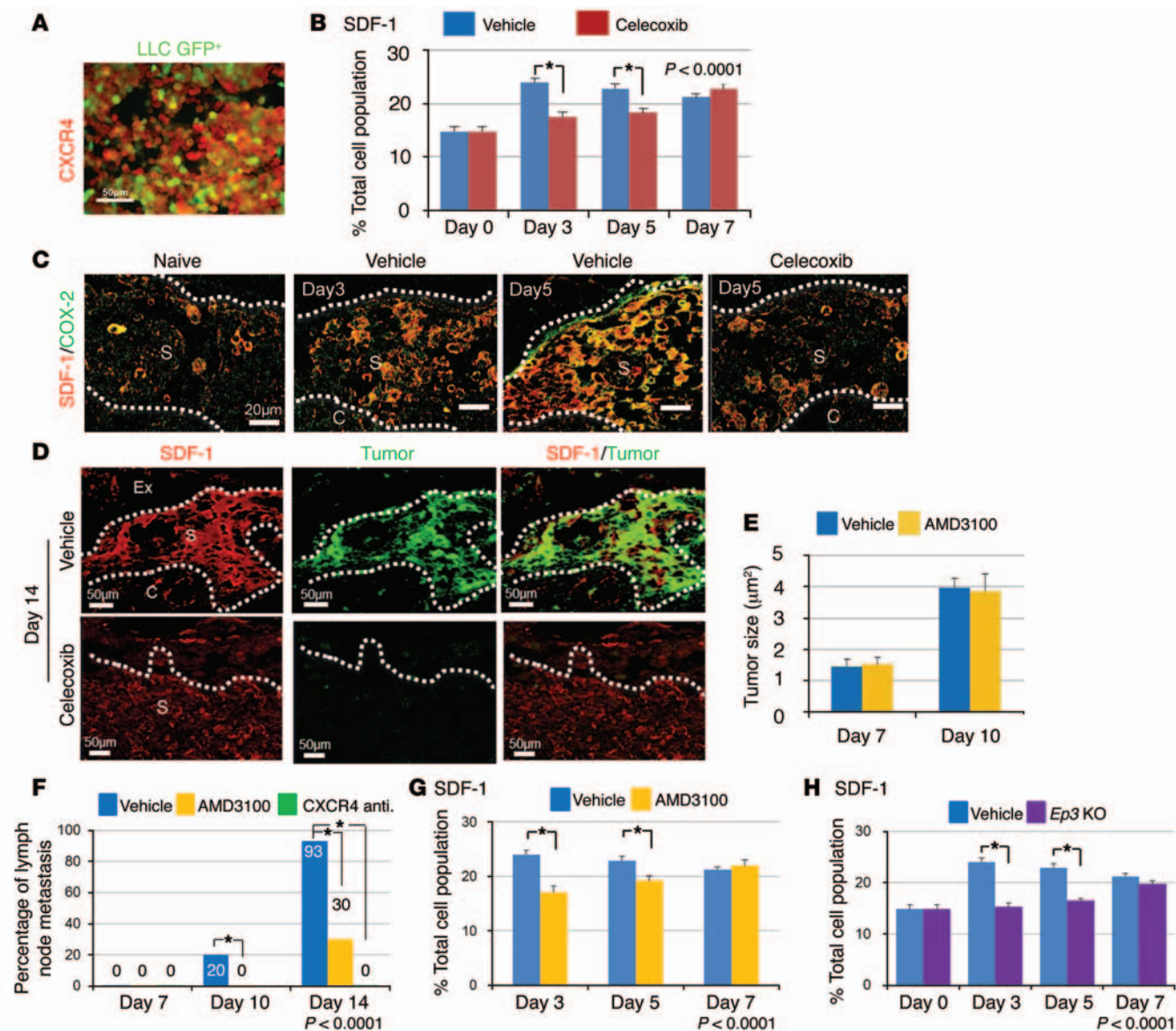


**Figure 2. COX-2/EP3 enhances SDF-1 expression in lymph nodes.** (A) Immunofluorescence images of CXCR4 in cultured GFP-positive LLC cells. Scale bar: 20  $\mu$ m. (B) SDF-1-positive cell population in the regional lymph nodes.  $n = 15$  per group.  $*P < 0.05$  ( $\chi^2$  test). (C) Immunofluorescence images showing COX-2/SDF-1 double staining in the regional lymph nodes. COX-2/SDF-1-double positive cells accumulated before arrival of GFP-negative LLC cells. Naive: Images from mice with no treatment. Scale bars: 50  $\mu$ m. (D) Accumulation of SDF-1/GFP-double positive LLC cells in subcapsular regions in regional lymph nodes at day 14. Celecoxib treatment reduced them. Scale bars: 50  $\mu$ m. (E) Temporal changes in tumor size from vehicle-treated mice and AMD3100-treated mice. Vehicle,  $n = 15$ ; AMD3100,  $n = 10$ . (F) Temporal changes in the percentage of regional LNM-positive mice. AMD3100 and a CXCR4 neutralizing antibody were given throughout the experimental period. Vehicle,  $n = 15$ ; AMD3100,  $n = 10$ ; CXCR4 neutralizing antibody,  $n = 5$ .  $*P < 0.05$  ( $\chi^2$  test). (G) Temporal changes in the SDF-1-positive cell population in the regional lymph nodes. Vehicle,  $n = 15$ ; AMD3100,  $n = 10$ .  $*P < 0.0001$  (ANOVA). Student's  $t$  test was used to evaluate significant differences at days 3 and 5 ( $P < 0.05$ ). (H) Temporal changes in the SDF-1-positive cell population in the regional lymph nodes. The results from *Ep3* KO mice were compared with those from WT mice. WT,  $n = 15$ ; *Ep3* KO,  $n = 5$ .  $*P < 0.0001$  (ANOVA),  $P < 0.05$  (Student's  $t$  test). Values are mean  $\pm$  SD.  $N$  indicates the number of mice tested. Ex, extracellular matrix; S, subcapsular regions; C, cortical regions.

Quantification of CD11c/IDO-positive cells revealed that the reduction in the accumulation of CD11c/IDO-positive cells by COX-2 inhibition, CXCR4 blockade, and lack of EP3 signaling began at day 5 or day 7 (Figure 3, E and F). The CD11c-positive cells were also positive for SDF-1 (Figure 3G), suggesting that DCs are sources of SDF-1 in the premetastatic niche.

Moreover, the expression of CCR7, important for the adhesion and chemotaxis of leukocytes and DCs toward lymph nodes, was also suppressed in celecoxib-treated mice and *Ep3* KO mice com-

pared with vehicle mice (Supplemental Figure 3C). This result indicated that the induction of DCs associated with LNM was dependent on COX-2-derived PGE<sub>2</sub>-EP3 signaling. To examine whether PGE<sub>2</sub> induces SDF-1 in DCs, we isolated immature myeloid DCs from the bone marrow and cultured them in the presence of PGs. The mRNA and protein levels of SDF-1 increased significantly following PGE<sub>2</sub> stimulation (Supplemental Figure 3, D and E). To identify the receptor mediating this action, we added EP agonists (EP1-EP4), which are highly selective for each receptor subtype.

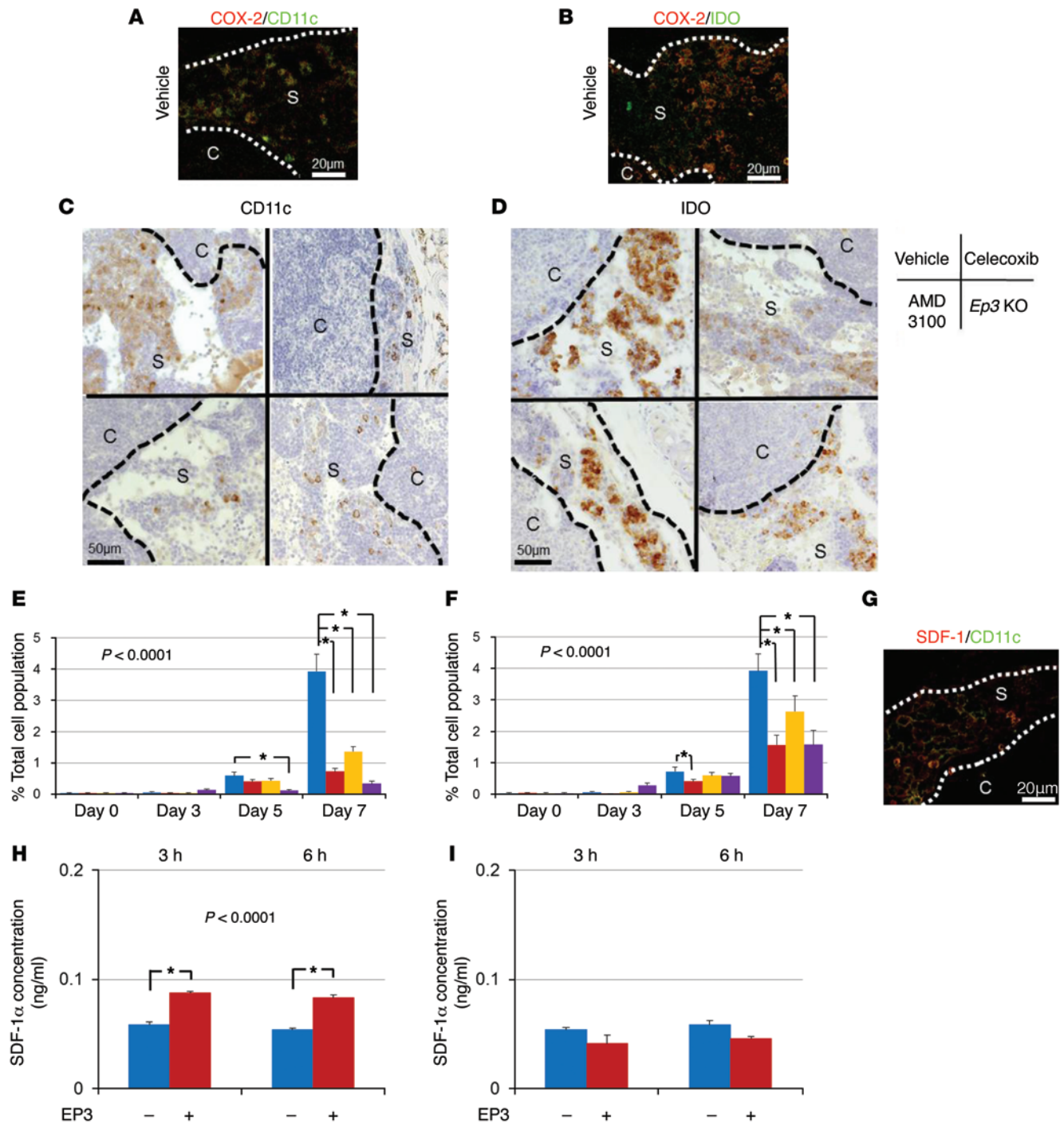


**Figure 3. Effect of the SDF-1/CXCR4 axis on LNM.** (A and B) COX-2/CD11c (A) and COX-2/IDO (B) double immunofluorescent staining of the subcapsular regions in regional lymph nodes at 7 days. Scale bars: 20  $\mu$ m. (C and D) Localization of CD11c-positive (C) and IDO-positive (D) cells in the subcapsular regions in regional lymph nodes at 7 days. Images are typical results from each group. Scale bars: 50  $\mu$ m. (E) Temporal changes in the CD11c-positive cell population in the regional lymph nodes. Vehicle,  $n = 15$ ; celecoxib,  $n = 15$ ; AMD3100,  $n = 10$ ; *Ep3* KO,  $n = 5$ .  $*P < 0.0001$  (ANOVA). Student's *t* test was used to evaluate significant differences at days 3, 5, and 7 ( $P < 0.05$ ). (F) Temporal changes in the IDO-positive cell population in the regional lymph nodes. Vehicle,  $n = 15$ ; celecoxib,  $n = 15$ ; AMD3100,  $n = 10$ ; *Ep3* KO,  $n = 5$ .  $*P < 0.0001$  (ANOVA). Student's *t* test was used to evaluate significant differences at days 3, 5, and 7 ( $P < 0.05$ ). (G) SDF-1/CD11c double immunofluorescence staining of the subcapsular regions in regional lymph nodes at 7 days. Scale bar: 20  $\mu$ m. (H) Induction of SDF-1 in cultured DCs by stimulation with an EP3 agonist. The level of SDF-1 in the culture medium was determined with a specific ELISA.  $n = 6$ .  $*P < 0.05$  (ANOVA). Student's *t* test was used to evaluate significant differences at each time point ( $*P < 0.05$ ). (I) SDF-1 levels in cultured DCs isolated from the bone marrow of *Ep3* KO mice. The experimental conditions were the same as those in H.  $n = 6$ . Error bars indicate the mean  $\pm$  SD. *N* indicates the number of mice tested. S, subcapsular regions; C, cortical regions.

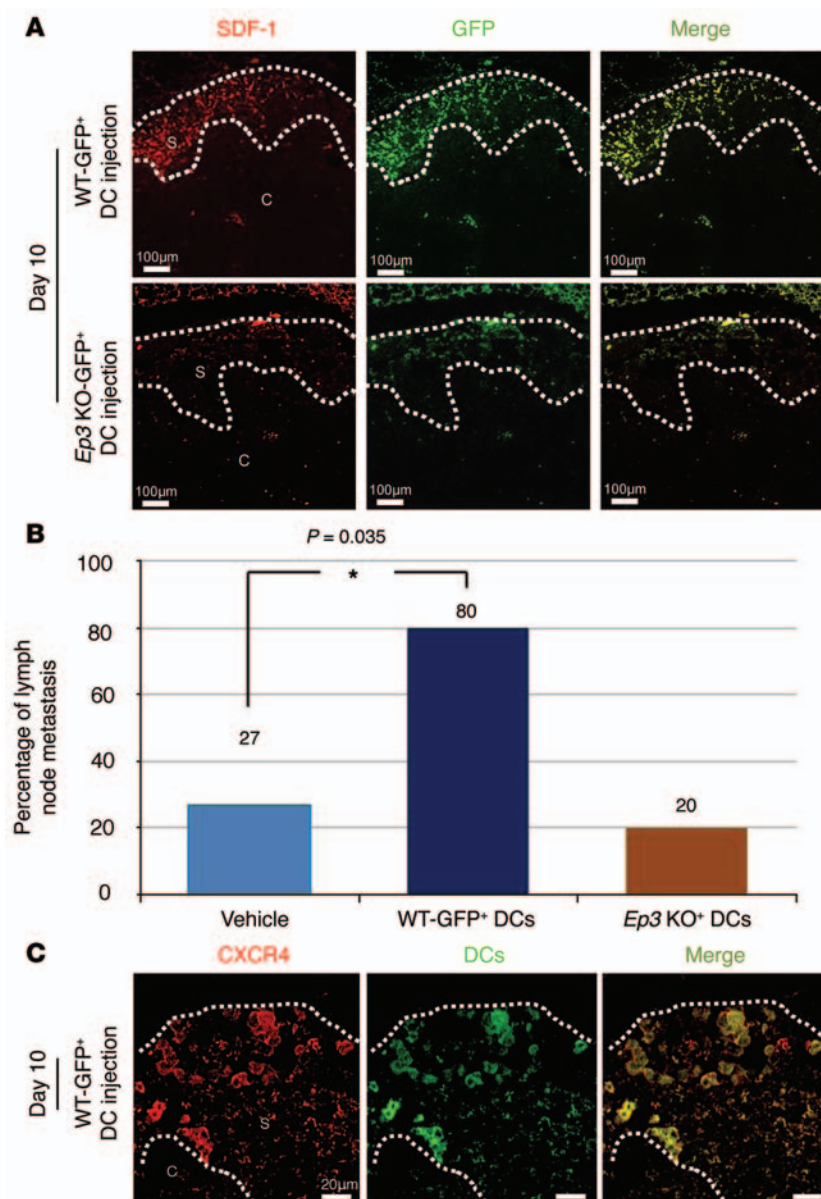


**Figure 4. COX-2-derived PGE<sub>2</sub>-EP3 signaling induces LNM and lymphangiogenesis by facilitating DC recruitment.** (A) Recruitment of DCs injected i.v. into the subcapsular regions of the regional lymph nodes. DCs were isolated from bone marrow cells derived from GFP transgenic WT mice and GFP transgenic *Ep3* KO mice. GFP-negative LLC cells were injected to the lungs of WT mice. Immunofluorescence images of SDF-1/GFP-double positive cells in the regional lymph nodes were taken at day 10. Scale bars: 100  $\mu$ m. (B) Percentage of LNM-positive mice receiving DCs from WT mice and *Ep3* KO mice. Injection of WT DCs facilitated LNM, whereas injection of *Ep3* KO DCs did not. *N* indicates the number of mice tested. Vehicle, *n* = 15; other groups, *n* = 5. \**P* = 0.035 ( $\chi^2$  test). (C) CXCR4 immunofluorescence images (taken at day 10) of the subcapsular regions of regional lymph nodes in WT mice receiving WT GFP-positive DCs. Many of the GFP-positive DCs were also CXCR4-positive. Scale bars: 20  $\mu$ m. S, subcapsular regions; C, cortical regions.

SDF-1 protein levels in the culture media increased upon incubation of DCs from WT mice with an EP3 agonist, ONO-AE-248 (Figure 3H); however, DCs from *Ep3* KO did not secrete SDF-1 (Figure 3I). Treatment with EP agonists for EP1, EP2, and EP4 did not increase SDF-1 secretion (Supplemental Figure 3F). These results suggested that DC accumulation in the premetastatic niche is dependent on COX-2/EP3 and SDF-1, and that induction of SDF-1 in DCs is dependent on EP3 signaling.

*EP3 signaling facilitates DC recruitment to the regional lymph node premetastatic niche.* To clarify the process of DC recruitment to the premetastatic niche, we injected mice i.v. with GFP-positive DCs following the injection of GFP-negative LLC cells. The GFP-positive DCs from WT mice were recruited to the subcapsular regions at day 10 (Figure 4A). This accumulation was significantly reduced following injection of GFP-positive DCs from *Ep3* KO mice (Figure 4A). In the early phase (premetastatic phase), DCs were recruited to subcapsular regions in an EP3 signaling-dependent manner too (Supplemental Figure 4, A and B). Furthermore, we estimated double staining by GFP and LYVE-1 in regional lymph nodes. GFP-positive DCs from WT mice (Supplemental Figure 4C) were significantly induced to LYVE-1-positive lymph vessels compared with GFP-positive DCs from *EP3* KO mice (Supplemental Figure 4D) at subcapsular regions of regional lymph nodes.

The WT DCs recruited to the subcapsular regions expressed higher levels of SDF-1 than those from *Ep3* KO mice. The percentage of LNM was higher following the injection of WT DCs than after the injection of vehicle or *Ep3* KO DCs (Figure 4B). Most of the accumulated DCs were CXCR4-positive (Figure 4C), suggesting that the DCs expressing EP3 enhanced the recruitment of DCs via the generation of SDF-1. These findings imply a positive-feedback loop in the EP3/SDF-1 interplay.

*Both COX-2-EP3 signaling and SDF-1 increase the recruitment of Tregs to the lymph node premetastatic niche.* Previous studies show that the increased production of PGE<sub>2</sub> by tumors is associated with the induction of Tregs and with T cell inhibition (29, 30). In the present study, we examined whether COX-2 inhibition could reduce Treg recruitment to the regional lymph nodes. As shown in Figure 5A, a substantial number of FOXP3<sup>+</sup> Tregs accumulated in the subcapsular regions of the regional lymph nodes; this accumulation was suppressed by celecoxib, AMD3100, and a lack of EP3 signaling. These results were confirmed by quantitative analysis (Figure 5B) and immunofluorescent analysis (Supplemental Figure 5, A and B). Taken together, these findings suggest that the accu-

mulumation of Tregs in lymph nodes is dependent on both COX-2/EP3 signaling and the SDF-1/CXCR4 axis. Since many of the FOXP3<sup>+</sup> cells expressed CXCR4 (Supplemental Figure 5C), it is possible that DC-derived SDF-1 may attract Tregs to the premetastatic niche. It was previously reported that immature DCs secrete TGF- $\beta$  to induce Treg proliferation (31). Therefore, to examine whether TGF- $\beta$ 1 was secreted by DCs in the premetastatic niche, we performed immunofluorescence analysis of TGF- $\beta$ 1 expres-

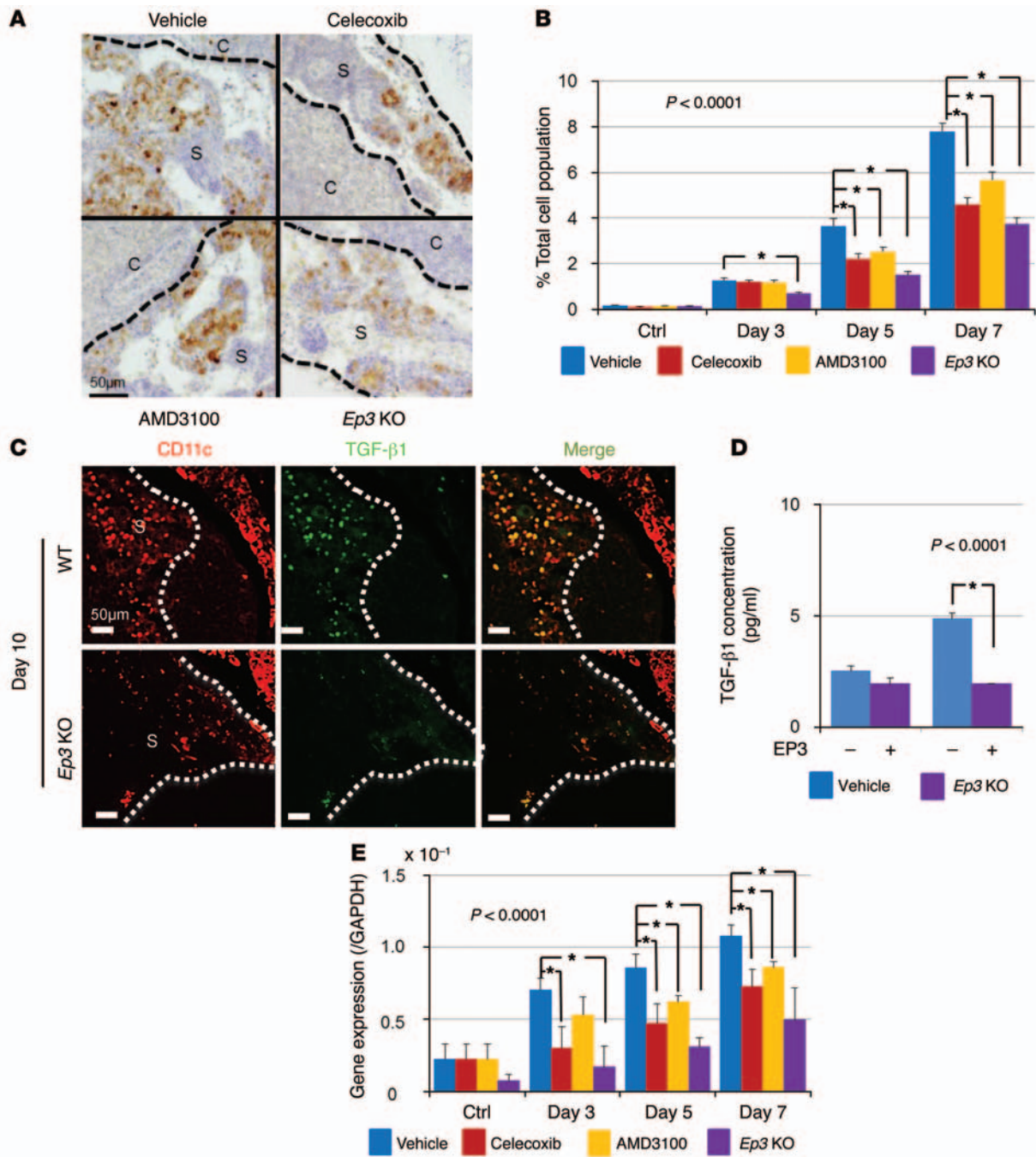


**Figure 5. COX-2-derived PGE<sub>2</sub>-EP3 signaling induces LNM by facilitating the accumulation of Treg cells.** (A) Localization of FOXP3-positive cells in the subcapsular regions in regional lymph nodes at 7 days. Images are typical results from each group. Scale bar: 50 μm. (B) Temporal changes in the FOXP3-positive cell population in the regional lymph nodes. Vehicle, n = 15; celecoxib, n = 15; AMD3100, n = 10; Ep3 KO, n = 5. \*P < 0.0001 (ANOVA). Student's t test was used to evaluate significant differences at days 3, 5, and 7 (P < 0.05). (C) CD11c/TGF-β1 immunofluorescence images in regional lymph nodes from WT mice and Ep3 KO mice at 10 days. The number of CD11c/TGF-β1-double positive cells was markedly reduced in Ep3 KO mice compared with that in WT mice. Scale bars: 50 μm. (D) TGF-β1 secretion by WT DCs and Ep3 KO DCs stimulated with an EP3 agonist (ONO-AE-248, 0.01 nM). The amount of immunoreactive TGF-β1 in the culture medium was determined by ELISA. n = 6. \*P < 0.05 (Student's t test). (E) Temporal changes in *Tgfb1* expression in the regional lymph nodes after LLC injection as determined by real-time PCR. Vehicle, n = 15; celecoxib, n = 15; AMD3100, n = 10; Ep3 KO, n = 5. \*P < 0.0001 (ANOVA), P < 0.05 (Student's t test). Error bars indicate the mean ± SD. N indicates the number of mice tested. S, subcapsular regions; C, cortical regions.

sion by CD11c-positive DCs. We found that CD11c-positive cells expressed TGF-β1 and that the number of CD11c/TGF-β1-double positive cells was reduced in Ep3 KO mice compared with that in WT mice (Figure 5C). We also measured TGF-β1 secretion by DCs cultured in the presence of an EP3 agonist. WT DCs secreted

large amounts of TGF-β1 in response to EP3 stimulation, but DCs from Ep3 KO mice did not (Figure 5D). TGF-β expression was significantly suppressed in celecoxib- or AMD3100-treated mice and in Ep3 KO mice (Figure 5E). These results suggested that the accumulation of Tregs in the premetastatic niche was COX-2/

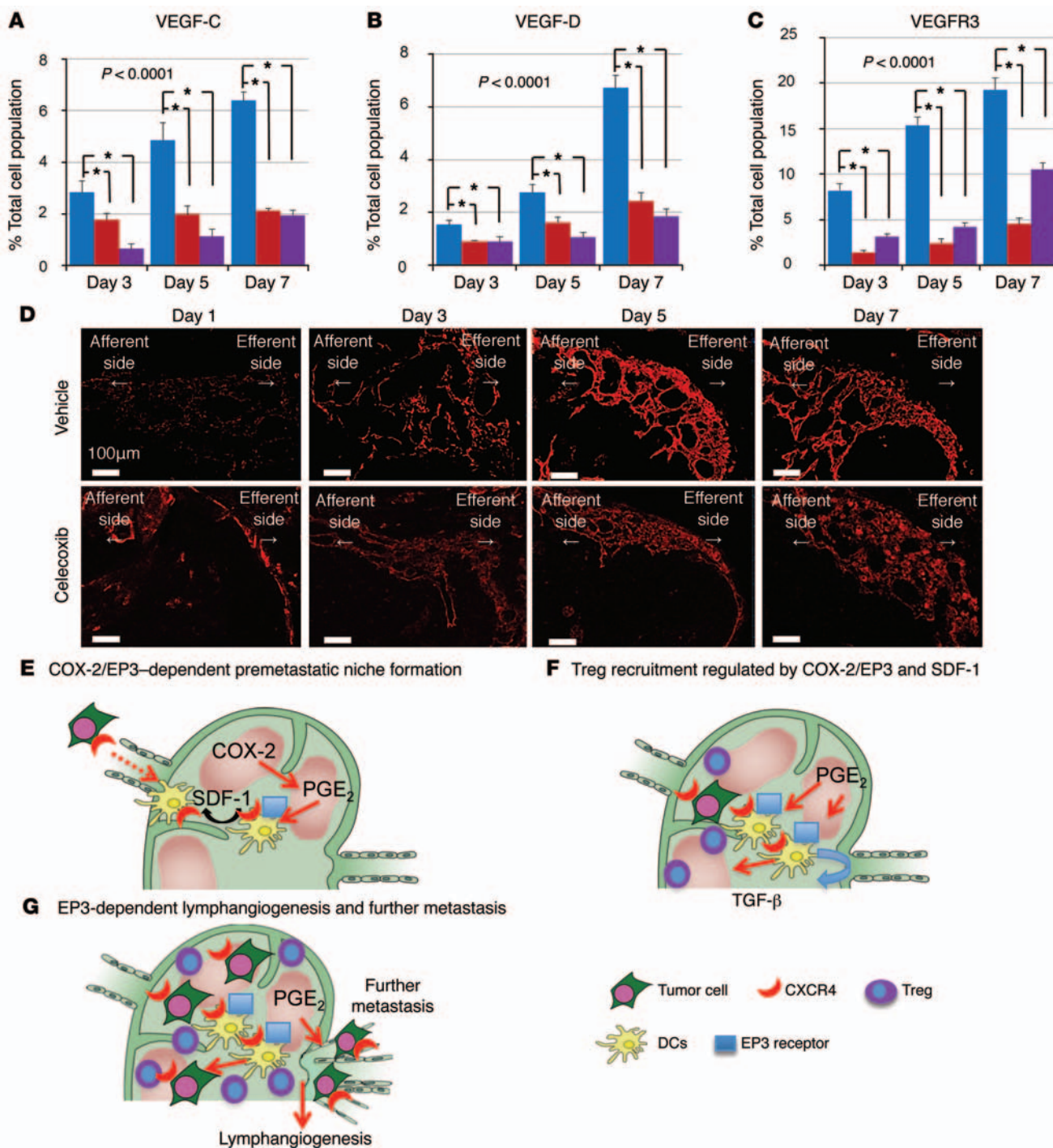


**Figure 6. COX-2-derived PGE<sub>2</sub>-EP3 signaling induces lymphangiogenesis.** (A–C) Temporal changes in the VEGF-C-positive cell (A), the VEGF-D-positive cell (B), and the VEGFR3-positive cell population (C) in the regional lymph nodes. *N* indicates the number of mice tested. Vehicle, *n* = 15; celecoxib, *n* = 15; *Ep3* KO, *n* = 5. Error bars indicate the mean  $\pm$  SD. \* $P < 0.0001$  (ANOVA). Student’s *t* test was used to evaluate significant differences at days 3, 5, and 7 ( $P < 0.05$ ). (D) Immunofluorescence images of regional lymph nodes stained with the LYVE-1 antibody. Lymphangiogenesis was observed at the efferent side of the regional lymph nodes in vehicle-treated mice from day 3, and was markedly reduced by celecoxib treatment. Scale bars: 100  $\mu$ m. (E) A schematic presentation of COX-2/SDF-1-dependent premetastatic niche formation. COX-2 and EP3 mediate the increase of SDF-1 at the premetastatic site before the arrival of tumor cells to the regional lymph node. CXCR4-positive tumor cells were mobilized to SDF-1-generating sites. Simultaneously, CXCR4/EP3-positive DCs are recruited to generate SDF-1 in response to EP3 signaling. (F) Tregs are recruited to the premetastatic niche via SDF-1/EP3 signaling. The DCs recruited to the premetastatic niche secrete TGF- $\beta$ 1 in an EP3/SDF-1-dependent manner. Thus, COX-2/PGE<sub>2</sub>-EP3 signaling together with SDF-1/CXCR4 signaling may decide the fate of the colonizing LLC cells. (G) Fate of metastasized tumor cells. COX-2/EP3 signaling upregulates lymph node lymphangiogenesis in the efferent side of the subcapsular region, and this facilitates tumor cell growth in the regional lymph nodes and lymph node or systemic metastasis.



EP3- and SDF-1/CXCR4-dependent, and that the accumulated Tregs might influence the fate of the tumor cells colonizing the premetastatic niche.

*PGE<sub>2</sub>-EP3 signaling as a regulator of lymph node lymphangiogenesis.* Once the metastatic cells arrive at the lymph nodes, lymph node lymphangiogenesis may facilitate further metastasis to other organs, such as the distal lymph nodes and lungs. It was reported that no metastases were observed in distant organs in the absence of lymph node metastases (32). We determined the expression of prolymphangiogenic growth factors, VEGF-C and VEGF-D, in the regional lymph nodes and found that the gene expression of these growth factors was significantly increased before the arrival of the LLC cells, but was suppressed in celecoxib-treated mice and in *Ep3* KO mice (Figure 6, A and B). Moreover, VEGFR3, expressed on lymphatic endothelial cells, was increased in the regional lymph nodes from day 3, but was reduced in celecoxib-treated mice and *Ep3* KO mice (Figure 6C). VEGF-C-, VEGF-D-, and VEGFR3-positive cells were costained against CD11b, a macrophage marker, and CD11c in the efferent side of subcapsular regions and analyzed by immunofluorescence (Supplemental Figure 6, A and B). These results suggested that COX-2/PGE<sub>2</sub>-EP3-dependent induction of VEGF-C/D in macrophages and DCs induces lymphangiogenesis in the efferent side of subcapsular regions. Furthermore, the size of regional lymph nodes and lymph vessel area were suppressed in *Ep3* KO mice and celecoxib-treated mice compared with vehicle-treated mice ( $P < 0.05$ , ANOVA; Figure 6D and Supplemental Figure 7, A and B). In contrast, there were no significant differences among vehicle- and celecoxib-treated mice and *Ep3* KO mice in primary lesion (Supplemental Figure 7C). These results suggested that PGE<sub>2</sub>-EP3 signaling induces lymphangiogenesis in regional metastatic lymph nodes before the arrival of LLC cells.

## Discussion

Our study demonstrates that the formation of the premetastatic niche in regional lymph nodes is dependent on COX-2/PGE<sub>2</sub>-EP3 signaling, and that SDF-1-expressing DCs have a significant effect on the accumulation of CXCR4-expressing LLC cells. COX-2/EP3-dependent induction of chemokine was initiated from the early stage in which there is no metastasis in regional lymph nodes. During these steps, there was no significant difference in primary tumor size under COX-2 inhibition and EP3 receptor knockout. EP3 signaling was also active to accumulate DCs in subcapsular regions of lymph nodes for future accumulation of LLC cells. We observed an increase in the release of SDF-1 from DCs in lymph nodes following LLC cell injection. In addition, we observed significant Treg recruitment to the premetastatic niche; this process was dependent on COX-2/EP3 and SDF-1. Lymph node lymphangiogenesis, which may facilitate further metastasis, was also induced in a COX-2/EP3-dependent manner. These findings indicate that prostanoid signaling plays a significant role in LNM.

Prostanoids, including prostaglandins, are generated from arachidonic acid, a process regulated by the rate-limiting COX enzymes. COX-2 can be induced in most tissues, where it mediates the production of proinflammatory PGs during inflammation and in tumorigenic settings. Neoplastic tissues, such as human colon cancers, contain high concentrations of PGs, and the protumorigenic effects of COX-2 are largely attributed to its role in PGE<sub>2</sub>

production (8). COX-2 expression is associated with poor patient prognosis and survival (33, 34). We previously reported that, in addition to tumor COX-2 expression, COX-2 present in stromal tissues had a significant effect on tumor-associated angiogenesis (35). Further studies showed that COX-2 induced lung metastasis via EP3 signaling (14). Iwata et al. previously reported that COX-2 inhibitor suppressed tumor lymphangiogenesis and LNM by using a gastric carcinoma cell line (36); however, little is known about the involvement of COX-2 and PG receptors in forming the premetastatic niche during LNM. The current study confirmed the report and revealed that COX-2 and EP3 signaling play a role in LNM, and showed that COX-2 and EP3 signaling mediate the induction of SDF-1 and CXCR4 to establish the premetastatic niche.

The cellular components involved in the formation of premetastatic niches are largely unknown. In the present study, we showed that DCs play an important role in the formation of the lymph node premetastatic niche. DCs are bone marrow-derived cells that are present in all tissues (37, 38). Lymph output of DCs in the steady state, continual traffic of DCs from peripheral tissue, is constant and is further augmented during inflammatory conditions (39, 40).

Mouse models of cancer reveal that DCs capture tumor antigens released from tumor cells and cross-present these antigens to T cells in the tumor-draining lymph nodes, thereby generating tumor-specific cytotoxic T lymphocytes, which play a role in tumor rejection (41, 42). DCs sample the environment and transmit the gathered information to cells of the adaptive immune system (T cells and B cells). DC differentiation from hematopoietic stem cells and DC function are sensitive to lipid mediators, such as PGs, and DCs express several receptors involved in PG signaling pathways (43). PGE<sub>2</sub> is a key modulator of DC differentiation, maturation, migration, and cytokine production (44–48). In contrast to its inhibitory effects on monocytes, PGE<sub>2</sub> activates immature DCs. As a first step toward the transition from an adhesive to a highly migratory state, DCs lose their specific integrin- and actin-rich adhesive structures, called podosomes, within minutes following PGE<sub>2</sub> stimulation (47). This rapid response to PGE<sub>2</sub> is mediated by increased intracellular levels of cAMP, activation of the small GTPase RhoA, and subsequent induction of actomyosin contraction, ultimately leading to rapid podosome dissolution (48). In the present study, we identified a novel function of DCs in premetastatic niche formation in the regional lymph nodes in tumor-bearing mice. As shown in Figure 3, A and B, COX-2 induction in DCs was observed at the early stages of the experiment, suggesting that COX-2 might regulate the formation of the premetastatic niche in the regional lymph nodes. SDF-1 induction in DCs was dependent on COX-2 and EP3 signaling, and blockade of the SDF-1/CXCR4 axis suppressed the formation of the premetastatic niche.

The chemokine receptor CCR7 is known as important for the adhesion and chemotaxis of leukocytes and DCs toward lymph nodes. Forster et al. reported that DC migration to lymph nodes was strictly dependent on CCR7 and its ligand in both the steady state and inflammation, and accordingly *Ccr7* KO DCs failed to migrate to lymph nodes. Thus, by bringing together T cells, B cells, and DCs to form functional microenvironments in secondary lymphoid organs, CCR7 has been identified as a major homing receptor and important regulator for initiating an antigen-specific

immune response (49, 50). The association of COX-2 and CCR7 with LNM of breast cancer has been already reported (51). In the current study the expression of CCR7 in regional lymph nodes was suppressed in celecoxib-treated mice compared with vehicle-treated mice. This result showed the possibility that COX-2-derived PGE<sub>2</sub> may induce DC migration that depends on CCR7.

FACS analysis was useful for characterizing and quantitating cell subsets in lymph nodes. Though we performed FACS for regional lymph nodes with the IntraStain FACS kit, we could not detect and obtain the expected results. As a substitution for this FACS analysis, we picked up mediastinal lymph nodes from the vehicle group and the *Ep3* KO group at 5 days and sorted CD11c-positive cells by FACS after homogenization; when we assayed the sorted cells for *Cox2* and *Sdf1* by RT-PCR, the message of COX-2 and SDF-1 was significantly suppressed in the *Ep3* KO group compared with the vehicle-treated group (Supplemental Figure 3, A and B). We thought that the quantitative analysis by RT-PCR was more sensitive, and we could substitute it for FACS analysis.

In vitro assays using isolated DCs showed that EP3 signaling upregulated SDF-1 expression (Figure 3, H and I). These findings revealed the crucial role of COX-2 and EP3 signaling in the formation of a premetastatic niche via the SDF-1/CXCR4 chemokine axis. The significance of EP3 signaling for DCs can be tested in mice with DC-specific conditional knockout. Use of *Tp<sup>fl/fl</sup>* mice in combination with *Cd11c-Cre* mice will provide a good opportunity to test the function of EP3 in DCs. At present, there is no good marker for DCs besides CD11c. But CD11c is expressed on other types of cells than DCs. We expect more suitable approaches to test DC-specific inhibition of EP3 signaling that regulates premetastatic niche formation.

We further demonstrated that Tregs were recruited to the regional lymph nodes via COX-2/EP3 and SDF-1. Tregs, formerly known as suppressor T cells, are a subpopulation of T cells that modulate the immune system, maintain tolerance to self-antigens, and abrogate the development of autoimmune disease (52). Studies in mouse models revealed the potential of Tregs for the treatment of autoimmune diseases and cancer, and for organ transplantation. Tregs were selectively recruited within lymphoid infiltrates and activated by mature DCs, likely through the recognition of tumor-associated antigen presentation, resulting in the prevention of effector T cell activation, immune escape, and, ultimately, tumor progression (53). Mansfield et al. reported that FOXP3<sup>+</sup> cells were associated with more advanced disease in breast cancer, a finding that is proven to be true in many other cancers (54). DCs have been found to promote Treg differentiation and may become a suitable target to abrogate the development of T cell tolerance and to promote an effective immune response to breast cancer (54). As shown in Figure 5B, the recruitment of Tregs was observed in the regional lymph node premetastatic niche, and it was suppressed by COX-2 inhibition, EP3 blockade, and SDF-1 blockade. To our knowledge, this is a novel finding, showing the interplay between prostanoids and Tregs. Tregs expressed CXCR4 (Supplemental Figure 4D); thus, SDF-1 secreted by DCs may act as a major attractant of Tregs to the premetastatic niche. This may increase the immunosuppressive potential of Tregs and facilitate further metastasis.

Furthermore, TGF- $\beta$ , which is a kind of cytokine produced by Tregs, has been implicated in tumor progression. The TGF- $\beta$  path-

way has been implicated in many of these metastatic processes and has been shown to dramatically impact the ability of tumor cells to spread throughout the body (55–58).

We previously reported that lymphangiogenesis in a Matrigel subcutaneous implantation model, which mimics tumor stromal reactions, was enhanced by COX-2 and EP3/4 signaling (12). In addition, topical implantation of both VEGF-C- and VEGF-A-overexpressing tumor cells induced lymphangiogenesis in sentinel lymph nodes (32). However, a more precise evaluation of lymph node lymphangiogenesis showed that lymphangiogenesis took place in the efferent lymphatic area (Figure 6D), whereas the premetastatic niche was formed in the subcapsular regions of the sentinel lymph nodes. The positive cells of prolymphangiogenic factors are tumor cells, macrophages, and DCs. Supplemental Figure 6 shows that VEGF-C-, VEGF-D-, and VEGFR3-positive cells, accumulated in the efferent side of lymph nodes, were positive for CD11b and CD11c. Those results suggested that lymphangiogenesis induced by CD11c-positive and CD11b-positive cells was dependent on COX-2/PGE<sub>2</sub>-EP3 signaling. We previously reported that PGE<sub>2</sub> stimulated the induction of VEGF-A/ C, and that VEGF-A induced COX-2 (12, 59–61). COX-2/EP3-dependent induction of SDF-1 in DCs localized in subcapsular regions may induce formation of the premetastatic niche for future colonization by LLC cells. It will be important to determine the exact mechanisms by which lymph node lymphangiogenesis induces further tumor cell metastasis to the lymph nodes and other tissues. Although the induction of lymph node lymphangiogenesis and subsequent DC motility following adjuvant-induced skin inflammation has been described (62), our study demonstrated that COX-2-positive SDF-1-producing DCs are the major cell component driving niche formation, whereas PGs regulate lymph node lymphangiogenesis. Lymph node lymphangiogenesis may decide the fate of the colonizing tumor cells, and blockade of PG biosynthesis and receptor signaling may prevent further tumor cell metastasis to the lymph nodes and other tissues.

In conclusion, our study shows that endogenous COX-2-derived PGE<sub>2</sub> stimulated the EP3 receptor on DCs, leading to the upregulation of SDF-1 expression in the subcapsular regions in regional lymph nodes following LLC cell injection into the lungs. SDF-1 upregulation facilitated the accumulation of CXCR4<sup>+</sup> LLC cells and the formation of the regional lymph node premetastatic niche (Figure 6E). We also found that accumulation of Tregs and lymph node lymphangiogenesis, both of which may decide the fate of metastasized tumor cells, were COX-2/EP3-dependent (Figure 6, F and G). Taken together, our findings suggest that PGE<sub>2</sub> inhibitors, together with SDF-1 receptor antagonists and EP3 antagonists, may be promising agents for the suppression of premetastatic niche formation and LNM.

## Methods

Supplemental Methods are available online with this article; doi:10.1172/JCI73530DS1.

**Cell lines.** LLC cells (cell number LL/2 [LLC1] [ATCC CRL-1642]) originally isolated from C57BL/6 mice were cultured at 37°C in DMEM (Gibco; Life Technologies) supplemented with 10% FBS (Gibco; Life Technologies) in a humidified atmosphere containing 5% CO<sub>2</sub>. LLC cells were purchased from Riken BioResource Center Cell Bank (RBRV-RCB2638).

**Retroviral transfection of GFP gene.** Murine GFP cDNA was cloned into a deficient retroviral vector pLEGFP (Clontech; Takara), then transfected into PT67 cells (Clontech; Takara), followed by G418 (Roche) selection. The resulting temporary infectious recombinant virus containing GFP was infected into NIH/3T3 cells, followed by G418 selection in order to evaluate the infectious titer of those viruses, and the resulting titer was approximately  $1 \times 10^3$  CFUs/ml. LLC cells were infected with these temporary infectious retroviruses and selected with G418, then designed as LLC-GFP.

**Animals and drugs.** Male C57BL/6 mice, 6–8 weeks old and weighing 20–25 g, were obtained from CLEA Japan. *Ep3* KO mice on a C57BL/6 hybrid background were generated by our research group. The mice (male, 8 weeks old) were maintained at a constant humidity ( $60\% \pm 5\%$ ) and temperature ( $20^\circ\text{C} \pm 1^\circ\text{C}$ ) and were kept continuously on a 12-hour light/dark cycle. All animals were provided with food and water ad libitum.

A COX-2 inhibitor, celecoxib (100 mg/kg per day; Pyser), and a CXCR4 antagonist, AMD3100 (10 mg/kg per day; Sigma-Aldrich), were administered orally every day. A CXCR4 neutralizing antibody (10 mg per mouse; clone 2B11; BD Biosciences) was injected i.p. daily. On days 3, 5, 7, 10, and 14, WT and *Ep3* KO mice were sacrificed using ether, and the lungs were resected. The isolated lungs were fixed with 4% PFA or 10% formalin, and analyzed under a microscope.

**Intrapulmonary implantation model.** Log-phase cell cultures of LLC-GFP cells were suspended at a cell density of  $5 \times 10^4$  per milliliter in 10  $\mu\text{l}$  PBS containing 10  $\mu\text{l}$  of Matrigel (Becton Dickinson Labware), and were injected into the mouse left lung parenchyma under anesthesia by ether. A small skin incision to the left chest wall (approximately 5 mm in length) was made at about 5 mm tail side from the scapula. A 30-gauge needle attached to a 0.5-ml insulin syringe was directly inserted through the intercostal space into the left lung to a depth of 2–3 mm. After implantation, the skin incision was closed with a surgical suture. To prevent bleeding after injection, a cotton-tipped applicator was pressed on the site of puncture. We performed this method very carefully and got very good reproducibility, and tumors developed at the site of implantation in 95% of animals.

**Fluorescence microscopy.** Mice were anesthetized as described above, and the integrity of the lymphatic vasculature of the tail was examined by fluorescence microlymphangiography. The filling of the lymphatic vasculature was monitored for 30 minutes under a fluorescence microscope (LSM710; Carl Zeiss) with equal exposure times for each mouse. The arbitrary units of fluorescence intensity were analyzed with ZEN2009 (Carl Zeiss) and were compared between the 2 groups.

**Immunofluorescence.** For immunofluorescence cytochemistry, lung tissues were immediately fixed with 4% paraformaldehyde in 0.1 mol/l phosphate buffer solution (pH 7.4). After fixation, the tissues were dehydrated with graded ethanol series and then embedded in paraffin. Sections of the paraffin-embedded tissues (4 mm thick) were mounted on glass slides, deparaffinized with xylene, and placed in  $4^\circ\text{C}$  acetone. The sections were blocked with 1% BSA-PBS and incubated with goat anti-mouse VEGF-C (1:200; Santa Cruz Biotechnology), goat anti-mouse VEGF-D (1:200; Santa Cruz Biotechnology), rabbit anti-mouse VEGFR3 (1:200; Santa Cruz Biotechnology), goat anti-mouse COX-2 (1:500; Abcam), rat anti-mouse stromal cell-derived factor-1 (SDF-1) (1:50; Santa Cruz Biotechnology), C-X-C receptor type 4 (CXCR4) (1:50; BD Pharmingen), rabbit anti-mouse IDO

(1:200; Santa Cruz Biotechnology), ArHm anti-mouse CD11c (1:200; Abcam), rat anti-mouse CD11b (1:100; AbD Serotec), mouse anti-mouse FOXP3 (1:500; eBioscience), and rabbit anti-mouse TGF- $\beta$  (1:200; Abcam) antibodies. After washing in PBS, the sections were incubated with Alexa Fluor 488 goat anti-rabbit IgG (1:200; Invitrogen, Life Technologies) and Alexa Fluor 568 goat anti-rat IgG (1:200; Invitrogen, Life Technologies) or incubated with Universal DAKO LSAB+ system-HRP (DAKO) with DAB and Mayer's hematoxylin solution. Negative control staining was performed by replacement of the primary antibodies with 1% BSA-PBS. Images were captured with a confocal scanning laser microscope (LSM710; Carl Zeiss) or a BX51 microscope (Olympus).

**Calculation of percentage total cell population.** The ratio of immunohistochemistry-positive cells for each antibody per field required for each point varies with the size of the high-power field ( $\times 400$ ) for a given microscope at regional lymph nodes by ImageJ software.

**Quantitative RT-PCR analysis.** The excised tissue samples were immediately immersed in RNeasy RNA Stabilization Reagent (QIAGEN), and homogenized for 60 seconds at 200 g using a Mag-NALyser (Roche). Harvested cells were washed 3 times with PBS solution and homogenized using a QIA Shredder (QIAGEN). Total RNA was extracted from the homogenized tissues and cells using the RNeasy Mini Kit (QIAGEN), and single-stranded cDNA was generated from 1  $\mu\text{g}$  of total RNA via reverse transcription using ReverTra Ace (TOYOBO Co. Ltd.), according to the manufacturer's instructions. Quantitative PCR amplification was performed using SYBR Premix Ex Taq (Takara Bio Inc.). The RT-PCR primers for *Cox2*, *Tgfb*, *Sdf1*, *Vegfc*, *Vegfd*, and *Vegfr3* were designed using Primer3 software (<http://primer3.sourceforge.net>) on the basis of data obtained from GenBank. The following primers were used for real-time RT-PCR: *Gapdh* forward 5'-ACATCAAGAAGGTGGTGAAGC-3', reverse 5'-AAGGTGGAAGAGTGGGAGTTG-3'; GFP sense 5'-ACTACAA-CAGCCACAACGTCT-3', antisense 5'-GGTGTCTGCTGGTAGTG-GTC-3'; COX-2 sense 5'-TGGGTGTGAAGGAAATAAGG-3', antisense 5'-CATCATATTTGAGCCTTGGGG-3'; SDF-1 sense 5'-CAGAGCCAACGTCAAGCA-3', antisense 5'-AGGTACTCTTG-GATCCAC-3'; TGF- $\beta$  sense 5'-AACAATTCCTGGCGTTACCTT-3', antisense 5'-TGTATTCCGTCTCCTTGGTTC-3'; VEGF-C sense 5'-TCTGTGTCCAGCGTAGATGAG-3', antisense 5'-GTCCCT-GTCCCTGGTATTGAG-3'; VEGF-D sense 5'-CCTATTGACATGCT-GTGGGAT-3', antisense 5'-GTGGGTTCTGGAGGTAAGAG-3'; VEGFR-3 sense 5'-TTTATGTCCCACCCCACTAC-3', antisense 5'-GGCTGAGCTACAAGGGCAATCG-3'; CCR7 sense 5'-TACATC-GCCGAGAATACCACG-3', antisense 5'-ATACATGAGAGGCAG-GAACCA-3' (Sigma-Aldrich).

**Bone marrow transplantation.** Bone marrow transplantation was performed as previously described (63). Donor bone marrow cells from *Ep3* KO mice and their WT counterparts were harvested, and the bone marrow mononuclear cells from each donor ( $2.0 \times 10^6$  cells in 200 ml PBS) were injected into the tail veins of WT mice irradiated with 9.0 Gy using an MBR-1505R X-ray irradiator (Hitachi Medical Co.) with a filter (copper, 0.5 mm; aluminum, 2 mm), while the cumulative radiation dose was monitored.

**Bone marrow-derived DCs and cell culture.** Bone marrow cells were isolated from the femur and tibia of donor male GFP transgenic WT or GFP-positive *EP3* KO mice (a gift from M. Okabe, Genome Information Research Center, Osaka University, Osaka, Japan). GFP-positive

and *Ep3* KO DCs were prepared from the mice by cross-breeding of GFP transgenic mice and *Ep3* KO mice. The cells were cultured ( $1 \times 10^6$  cells/ml, 5 ml/well) in GM-CSF-containing DMEM supplemented with 10% FBS at 37.1°C in 5% humidified CO<sub>2</sub> as previously described (64). The culture medium was changed every day to remove nonadherent granulocytes. On day 8, cells were harvested by light pipetting. More than 90% of the cells expressed CD11c by FACS analysis. DCs were stimulated with PGE<sub>2</sub> (0.1 nM per well) for 3, 6, and 24 hours.

**In vitro SDF-1 and TGF- $\beta$ 1 expression.** To assess DCs' expression of SDF-1 and TGF- $\beta$ 1 in vitro, DCs were stimulated with PGE<sub>2</sub> and EP1-EP4 agonists for 3, 6, and 24 hours in serum-free medium. The culture medium was collected and stored at -20°C until analysis. The medium was used to assess SDF-1 and TGF- $\beta$ 1 levels using specific ELISA kits (R&D Systems). ELISA kits were also used to measure SDF-1 and TGF- $\beta$ 1 levels in the cell culture supernatants. This experiment was performed in duplicate of serum-free medium.

**Statistics.** Data are expressed as the means  $\pm$  SD. Comparisons between multiple groups were performed by ANOVA followed by Scheffe's test. Comparisons between 2 groups were made by 2-tailed Student's *t* test. The correlation between the number of DCs and metastasis was analyzed using the  $\chi^2$  test. *P* < 0.05 was considered statistically significant.

**Study approval.** Animal studies were approved by the local ethics committee, and all experiments were performed in accordance with the guidelines for animal experiments of Kitasato University School of Medicine.

## Acknowledgments

We thank Mieko Hamano, Michiko Ogino, and Kyoko Yoshikawa for their technical assistance, Masato Saegusa and Miki Hashimura for their suggestions on pathological technique, and Makoto Murakami and Yoshitaka Taketomi (Tokyo Metropolitan Institute of Medical Science) for their suggestions on FACS experiments. This work was supported by grants from the Ministry of Education, Culture, Sports, Science and Technology, 23116102, 24659119, 26462132, and 26293055; Kitasato University Research Grant for Young Researchers; a grant from the Takeda Science Foundation; and a grant from Kitasato University Graduate School of Medical Sciences (Integrative Research Program 2013–2014).

Address correspondence to: Masataka Majima, Department of Pharmacology, Kitasato University School of Medicine, Kitasato 1-15-1, Minami-ku, Sagami-hara, Kanagawa 252-0374, Japan. Phone: 81427788822; E-mail: mmajima@med.kitasato-u.ac.jp.

- Pepper MS. Lymphangiogenesis and tumor metastasis: myth or reality? *Clin Cancer Res.* 2001;7(3):462–468.
- Paget S. The distribution of secondary growths in cancer of the breast. 1889. *Cancer Metastasis Rev.* 1989;8(2):98–101.
- Hiratsuka S, et al. The S100A8-serum amyloid A3-TLR4 paracrine cascade establishes a premetastatic phase. *Nat Cell Biol.* 2008;10(11):1349–1355.
- Kaplan RN, et al. VEGFR1-positive haematopoietic bone marrow progenitors initiate the premetastatic niche. *Nature.* 2005;438(7069):820–827.
- Kim M, et al. CXCR4 signaling regulates metastasis of chemoresistant melanoma cells by a lymphatic metastatic niche. *Cancer Res.* 2010;70(24):10411–10421.
- Wilson NS, Villadangos JA. Regulation of antigen presentation and cross-presentation in the dendritic cell network: facts, hypothesis, and immunological implications. *Adv Immunol.* 2005;86:241–305.
- Braun D, Longman RS, Albert ML. A two-step induction of indoleamine 2,3 dioxygenase (IDO) activity during dendritic-cell maturation. *Blood.* 2005;106(7):2375–2381.
- Greenhough A, et al. The COX-2/PGE2 pathway: key roles in the hallmarks of cancer and adaptation to the tumour microenvironment. *Carcinogenesis.* 2009;30(3):377–386.
- Sombroek CC, et al. Prostanoids play a major role in the primary tumor-induced inhibition of dendritic cell differentiation. *J Immunol.* 2002;168(9):4333–4343.
- Trinath J, et al. Intravenous immunoglobulin expands regulatory T cells via induction of cyclooxygenase-2-dependent prostaglandin E2 in human dendritic cells. *Blood.* 2013;122(8):1419–1427.
- Amano H, et al. Host prostaglandin E2-EP3 signaling regulates tumor-associated angiogenesis and tumor growth. *J Exp Med.* 2003;197(2):221–232.
- Hosono K, et al. Roles of prostaglandin E2-EP3/EP4 receptor signaling in the enhancement of lymphangiogenesis during fibroblast growth factor-2-induced granulation formation. *Arterioscler Thromb Vasc Biol.* 2011;31(5):1049–1058.
- Katoh H, et al. COX-2 and prostaglandin EP3/EP4 signaling regulate the tumor stromal proangiogenic microenvironment via CXCL12-CXCR4 chemokine systems. *Am J Pathol.* 2010;176(3):1469–1483.
- Amano H, et al. Roles of a prostaglandin E-type receptor, EP3, in upregulation of matrix metalloproteinase-9 and vascular endothelial growth factor during enhancement of tumor metastasis. *Cancer Sci.* 2009;100(12):2318–2324.
- Arya M, Ahmed H, Silhi N, Williamson M, Patel HR. Clinical importance and therapeutic implications of the pivotal CXCL12-CXCR4 (chemokine ligand-receptor) interaction in cancer cell migration. *Tumour Biol.* 2007;28(3):123–131.
- Sun X, et al. CXCL12/CXCR4/CXCR7 chemokine axis and cancer progression. *Cancer Metastasis Rev.* 2010;29(4):709–722.
- Teicher BA, Fricker SP. CXCL12 (SDF-1)/CXCR4 pathway in cancer. *Clin Cancer Res.* 2010;16(11):2927–2931.
- Zeelenberg IS, Ruuls-Van Stalle L, Roos E. The chemokine receptor CXCR4 is required for outgrowth of colon carcinoma micrometastases. *Cancer Res.* 2003;63(13):3833–3839.
- Bachelder RE, Wendt MA, Mercurio AM. Vascular endothelial growth factor promotes breast carcinoma invasion in an autocrine manner by regulating the chemokine receptor CXCR4. *Cancer Res.* 2002;62(24):7203–7206.
- Belperio JA, Phillips RJ, Burdick MD, Lutz M, Keane M, Strieter R. The SDF-1/CXCL12/CXCR4 biological axis in non-small cell lung cancer metastases. *Chest.* 2004;125(5):156S.
- Burger M, et al. Functional expression of CXCR4 (CD184) on small-cell lung cancer cells mediates migration, integrin activation, and adhesion to stromal cells. *Oncogene.* 2003;22(50):8093–8101.
- Singh S, Singh UP, Grizzle WE, Lillard JW, Lillard JW Jr. CXCL12-CXCR4 interactions modulate prostate cancer cell migration, metalloproteinase expression and invasion. *Lab Invest.* 2004;84(12):1666–1676.
- Scala S, et al. Expression of CXCR4 predicts poor prognosis in patients with malignant melanoma. *Clin Cancer Res.* 2005;11(5):1835–1841.
- Gentilini A, et al. Role of the stromal-derived factor-1 (SDF-1)-CXCR4 axis in the interaction between hepatic stellate cells and cholangiocarcinoma. *J Hepatol.* 2012;57(4):813–820.
- Uchida D, et al. Possible role of stromal-cell-derived factor-1/CXCR4 signaling on lymph node metastasis of oral squamous cell carcinoma. *Exp Cell Res.* 2003;290(2):289–302.
- Albrecht I, Christofori G. Molecular mechanisms of lymphangiogenesis in development and cancer. *Int J Dev Biol.* 2011;55(4):483–494.
- Burger JA, Kipps TJ. CXCR4: a key receptor in the crosstalk between tumor cells and their microenvironment. *Blood.* 2006;107(5):1761–1767.
- von Bergwelt-Baildon MS, et al. CD25 and indoleamine 2,3-dioxygenase are up-regulated by prostaglandin E2 and expressed by tumor-associated dendritic cells in vivo: additional mechanisms of T-cell inhibition. *Blood.* 2006;108(1):228–237.
- Baratelli F, et al. Prostaglandin E2 induces FOXP3 gene expression and T regulatory cell function in human CD4<sup>+</sup> T cells. *J Immunol.* 2005;175(3):1483–1490.
- Sharma S, et al. Tumor cyclooxygenase-2/prostaglandin E2-dependent promotion of FOXP3 expression and CD4<sup>+</sup> CD25<sup>+</sup> T regulatory cell activities in lung cancer. *Cancer Res.* 2005;65(12):5211–5220.
- Ghiringhelli F, et al. Tumor cells convert imma-

- ture myeloid dendritic cells into TGF- $\beta$ -secreting cells inducing CD4<sup>+</sup>CD25<sup>+</sup> regulatory T cell proliferation. *J Exp Med*. 2005;202(7):919–929.
32. Hirakawa S, Brown LF, Kodama S, Paavonen K, Alitalo K, Detmar M. VEGF-C-induced lymphangiogenesis in sentinel lymph nodes promotes tumor metastasis to distant sites. *Blood*. 2007;109(3):1010–1017.
  33. Khuri FR, et al. Cyclooxygenase-2 overexpression is a marker of poor prognosis in stage I non-small cell lung cancer. *Clin Cancer Res*. 2001;7(4):861–867.
  34. Peng L, Zhou Y, Wang Y, Mou H, Zhao Q. Prognostic significance of COX-2 immunohistochemical expression in colorectal cancer: a meta-analysis of the literature. *PLoS One*. 2013;8(3):e58891.
  35. Yoshida S, et al. COX-2/VEGF-dependent facilitation of tumor-associated angiogenesis and tumor growth in vivo. *Lab Invest*. 2003;83(10):1385–1394.
  36. Iwata C, et al. Inhibition of cyclooxygenase-2 suppresses lymph node metastasis via reduction of lymphangiogenesis. *Cancer Res*. 2007;67(21):10181–10189.
  37. Banchereau J, Steinman RM. Dendritic cells and the control of immunity. *Nature*. 1998;392(6673):245–252.
  38. Steinman RM, Banchereau J. Taking dendritic cells into medicine. *Nature*. 2007;449(7161):419–426.
  39. MacPherson GG, Jenkins CD, Stein MJ, Edwards C. Endotoxin-mediated dendritic cell release from the intestine. Characterization of released dendritic cells and TNF dependence. *J Immunol*. 1995;154(3):1317–1322.
  40. Pugh CW, MacPherson GG, Steer HW. Characterization of nonlymphoid cells derived from rat peripheral lymph. *J Exp Med*. 1983;157(6):1758–1779.
  41. Diamond MS, et al. Type I interferon is selectively required by dendritic cells for immune rejection of tumors. *J Exp Med*. 2011;208(10):1989–2003.
  42. Fuertes MB, et al. Host type I IFN signals are required for antitumor CD8<sup>+</sup> T cell responses through CD8 $\alpha$ <sup>+</sup> dendritic cells. *J Exp Med*. 2011;208(10):2005–2016.
  43. Gualde N, Harizi H. Prostanoids and their receptors that modulate dendritic cell-mediated immunity. *Immunol Cell Biol*. 2004;82(4):353–360.
  44. Khayrullina T, Yen JH, Jing H, Ganea D. In vitro differentiation of dendritic cells in the presence of prostaglandin E2 alters the IL-12/IL-23 balance and promotes differentiation of Th17 cells. *J Immunol*. 2008;181(1):721–735.
  45. Legler DF, Krause P, Scandella E, Singer E, Groettrup M. Prostaglandin E2 is generally required for human dendritic cell migration and exerts its effect via EP2 and EP4 receptors. *J Immunol*. 2006;176(2):966–973.
  46. Singh P, et al. Blockade of prostaglandin E2 signaling through EP1 and EP3 receptors attenuates Flt3L-dependent dendritic cell development from hematopoietic progenitor cells. *Blood*. 2012;119(7):1671–1682.
  47. van Helden SF, Krooshoop DJ, Broers KC, Raymakers RA, Figdor CG, van Leeuwen FN. A critical role for prostaglandin E2 in podosome dissolution and induction of high-speed migration during dendritic cell maturation. *J Immunol*. 2006;177(3):1567–1574.
  48. Van Helden SF, Oud MM, Joosten B, Peterse N, Figdor CG, van Leeuwen FN. PGE2-mediated podosome loss in dendritic cells is dependent on actomyosin contraction downstream of the RhoA-Rho-kinase axis. *J Cell Sci*. 2008;121(pt 7):1096–1106.
  49. Forster R, et al. CCR7 coordinates the primary immune response by establishing functional microenvironments in secondary lymphoid organs. *Cell*. 1999;99(1):23–33.
  50. Sallusto F, Lenig D, Forster R, Lipp M, Lanzavecchia A. Two subsets of memory T lymphocytes with distinct homing potentials and effector functions. *Nature*. 1999;401(6754):708–712.
  51. Pan MR, Hou MF, Chang HC, Hung WC. Cyclooxygenase-2 up-regulates CCR7 via EP2/EP4 receptor signaling pathways to enhance lymphatic invasion of breast cancer cells. *J Biol Chem*. 2008;283(17):11155–11163.
  52. Hori S, Nomura T, Sakaguchi S. Control of regulatory T cell development by the transcription factor Foxp3. *Science*. 2003;299(5609):1057–1061.
  53. Gobert M, et al. Regulatory T cells recruited through CCL22/CCR4 are selectively activated in lymphoid infiltrates surrounding primary breast tumors and lead to an adverse clinical outcome. *Cancer Res*. 2009;69(5):2000–2009.
  54. Mansfield AS, Heikkila PS, Vaara AT, von Smitten KA, Vakkila JM, Leidenius MH. Simultaneous Foxp3 and IDO expression is associated with sentinel lymph node metastases in breast cancer. *BMC Cancer*. 2009;9:231.
  55. Wels J, Kaplan RN, Raffii S, Lyden D. Migratory neighbors and distant invaders: tumor-associated niche cells. *Genes Dev*. 2008;22(5):559–574.
  56. Pollard JW. Tumour-educated macrophages promote tumour progression and metastasis. *Nat Rev Cancer*. 2004;4(1):71–78.
  57. Kalluri R, Zeisberg M. Fibroblasts in cancer. *Nat Rev Cancer*. 2006;6(5):392–401.
  58. Akhurst RJ, Derynck R. TGF-beta signaling in cancer — a double-edged sword. *Trends Cell Biol*. 2001;11(11):S44–S51.
  59. Amano H, Hayashi I, Ando K, Minamida S, Yoshimura H, Majima M. Adenylate cyclase/protein kinase A signaling pathway enhances angiogenesis through induction of vascular endothelial growth factor in vivo. *Jpn J Pharmacol*. 2002;88(3):179p–179p.
  60. Kashiwagi S, Hosono K, Suzuki T, Takeda A, Uchinuma E, Majima M. Role of COX-2 in lymphangiogenesis and restoration of lymphatic flow in secondary lymphedema. *Lab Invest*. 2011;91(9):1314–1325.
  61. Majima M, Hayashi I, Muramatsu M, Katada J, Yamashina S, Katori M. Cyclo-oxygenase-2 enhances basic fibroblast growth factor-induced angiogenesis through induction of vascular endothelial growth factor in rat sponge implants. *Br J Pharmacol*. 2000;130(3):641–649.
  62. Angeli V, et al. B cell-driven lymphangiogenesis in inflamed lymph nodes enhances dendritic cell mobilization. *Immunity*. 2006;24(2):203–215.
  63. Ogawa Y, et al. Bone marrow-derived EP3-expressing stromal cells enhance tumor-associated angiogenesis and tumor growth. *Biochem Biophys Res Commun*. 2009;382(4):720–725.
  64. Lutz MB, Kukutsch NA, Menges M, Rossner S, Schuler G. Culture of bone marrow cells in GM-CSF plus high doses of lipopolysaccharide generates exclusively immature dendritic cells which induce alloantigen-specific CD4 T cell anergy in vitro. *Eur J Immunol*. 2000;30(4):1048–1052.